# Sensor tntegration for the development of efficient, sustainable and more habitable cities

Alejandro Gallardo[1]
*Carleton College Department of Physics and Astronomy*

(Dated: 17 April 2019)

As urban migration and population density increase, cities experience exacerbated levels of traffic congestion, energy consumption, and polluted air. These issues can be tackled effectively with data driven solutions, allowing significant improvements for city efficiency, sustainability, and habitability.

This paper focuses on one method of gathering data: sensors. Magnetic field sensors can provide the data necessary for solutions that alleviate traffic and other major traffic inefficiencies. Phase sensors can facilitate bulk integration of renewable energies into the power grid. Finally, temperature profiling sensors can help detect wildfires at an early stage. Exploring how cities can use sensor technology will probe relevant physics and engineering topics within electronics, band theory, power grid energy flow, wave theory, and more.

## I. IMPROVING CITIES WITH DATA

According to the UN, an estimated 4.1 billion people live in cities in 2018, which is more than half of the world's current population. The number is rising very quickly as people move to cities—between 2010 and 2016, Minneapolis, Austin, Seattle and Denver grew by 8, 20, 16, and 15 percent respectively[1]. City populations are increasing so fast that the UN predicts 6.6 billion people will be living in cities by 2050[2].

As population and city migration increase, many of the issues cities face, such as traffic congestion and pollution, will be severely exacerbated[3]. In the city of Boston, each driver loses up to 7 days of their year stuck in peak hour traffic, costing the city 4.1 billion dollars annually. The situation in Boston is commonplace in US cities, and even worse for some cities like New York and LA[4]. Intensifying city congestion contributes to worsening levels of air pollution. It is ironic joggers who go for morning runs subject themselves to city air conditions that have been linked to respiratory illnesses, heart conditions, and cancer[5]. In addition, increasing city populations are contributing to the skyrocketing housing prices. The quantity and magnitude of issues hindering cities today is mind numbing, and will worsen as time progresses at society's business-as-usual.

Cities need to urgently pursue meaningful solutions to address these time sensitive problems. Data gathering allows us to detect and quantify issues, enabling many potentially powerful solutions. For example, if traffic lights could accurately detect vehicle congestion at an intersection, they could be programmed to dynamically switch scheduling such that it optimizes traffic flow. This would greatly reduce general congestion and the time sitting idle in front of a red light[6].

As shown in Fig. I, sensors form the foundational layer for creating meaningful applications, and can impact many domains such as agriculture, public security, healthcare, transportation and much more. In order to make the data gathered by sensors accessible, the sensors need to communicate with a central database or with each other. Once data is accessible, we can build applications targeting specific issues cities face today.

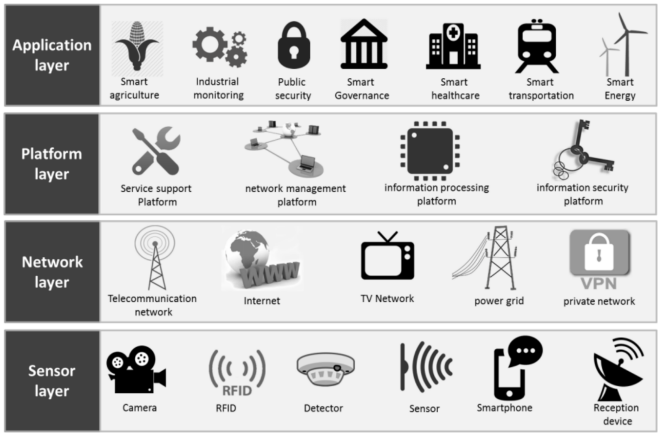


FIG. 1. Four layers of smart city[7]

## II. SMART TRANSPORTATION

According to the United States Department of Transportation, 10 percent of all traffic delay is due to inefficient traffic lights scheduled by timers. Similarly, 30 percent of traffic is caused by people looking for parking[8]. As will be explored, sensor based solutions can effectively reduce these inefficiencies in parking, traffic light scheduling, and much more.

Simply knowing where road-users are in real time can enable powerful solutions for traffic flow management. One method for detecting cars uses vehicles themselves as the source of real-time data. Currently, modern vehicles have a myriad of sensors, such as for coordinate location, wheel speed, motor position, visual sensing and more. By 2020, modern vehicles are expected to have over 200 sensors per vehicle— vehicles have increasingly rich local awareness! Aggregated vehicular data can provide a rich data set for vehicular detection.

This paper will focus on an alternative and more established method for vehicle detection: wireless sensor networks (WSNs). Vehicles can be detected through a network of sensors in which nodes are located in traffic light intersection and other relevant areas. Many different kinds of sensors have been considered and re-

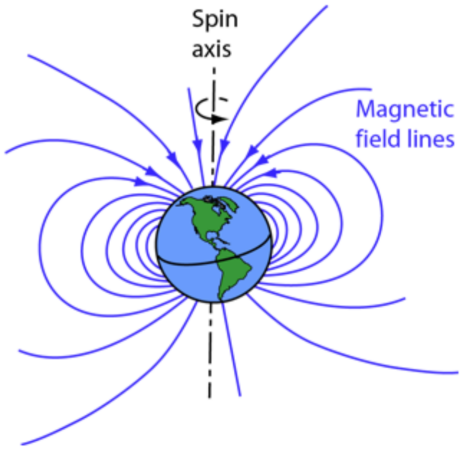


FIG. 2. Earth's magnetic field lines[11].

searched for the purpose of vehicle detection, such as cameras, inductive loops, piezoelectric sensors, and mobile crowdsensing[9]. Magnetic field sensors— also known as magnetometers— are among the most common sensor for WSNs since they generally have a lower cost for installation[10].

Magnetic field sensors can determine the presence of a metal object by measuring fluctuations in the magnetic field surrounding the sensor. As a result, we can use Earth's magnetic field to detect vehicle presence and motion. In order to see how, recall that according Maxwell's equations, magnetic field lines always form closed loops. Consequently, Earth's magnetic field lines are non-uniform, as shown in Fig. 2. However, at sufficiently small scales, Earth's magnetic field will appear uniform, as shown in Fig. 3. Due to Earth's locally uniform magnetic field, the ferromagnetic components of vehicles (i.e. wheels, engine, etc.) will become magnetized in the direction of Earth's magnetic field. Vehicles will produce non-uniform magnetic fields that will interfere with Earth's uniform magnetic field, as shown in Fig. 4. Therefore, vehicles will produce unique interference patterns depending on parameters such as size and shape. The interference can then be quantified using magnetometers.

There are a lot of different phenomenon allowing us to detect magnetic field fluctuations, including the Hall Effect, magneto-impedance, quantum interference— the list goes on. For vehicle detection, sensors that make use of Lorentz Forces and anisotropic magnetoresistance (AMR) are particularly practical[13].

### A. Lorentz Force Magnetometer

This section explores the physics of Lorentz Force Magnetometers in the context of using them to improve transportation efficiency in cities. The goal is to explore how the output voltage of the Lorentz Force Magnetometer is related to fluctuations in a magnetic field.


FIG. 3. Approximately what Earth's magnetic field looks like at sufficiently small scales.

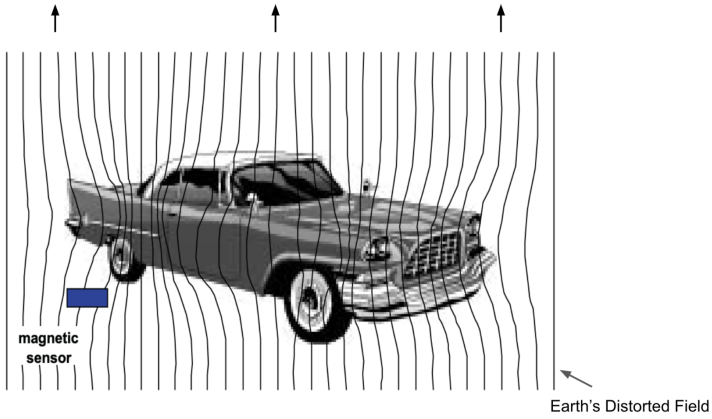


FIG. 4. A vehicle distorting Earth's uniform magnetic field due to ferromagnetic material in the vehicle. The variations in the magnetic field can be detected using a magnetic field sensor[12].

Lorentz Force sensors are micro-electromechanical systems (MEMS), which are systems that have several electronic and mechanical components that are in the micrometer scale. Fig. 5 shows a 3d image of what the device looks like. It is composed of three main components– 1) a large silicon substrate, which holds together the device; 2) a perforated plate that is attached to the substrate by a narrow support beam; 3) an aluminum trace outlining the perimeter of the perforated plate, which will carry current.

From electrodynamics, we know that current-carrying wire will experience Lorentz Forces when subject to a magnetic field. When subject to a magnetic field $\vec{B}$, a particle with charge q and velocity $\vec{v}$ will experience a Lorentz Force:

$$\vec{F} = q\vec{v} \times \vec{B} \tag{1}$$

By applying definitions for current, we can derive an expression that describes the Lorentz Force on a current-carrying wire:

$$\vec{F} = \vec{I}L \times \vec{B} \tag{2}$$

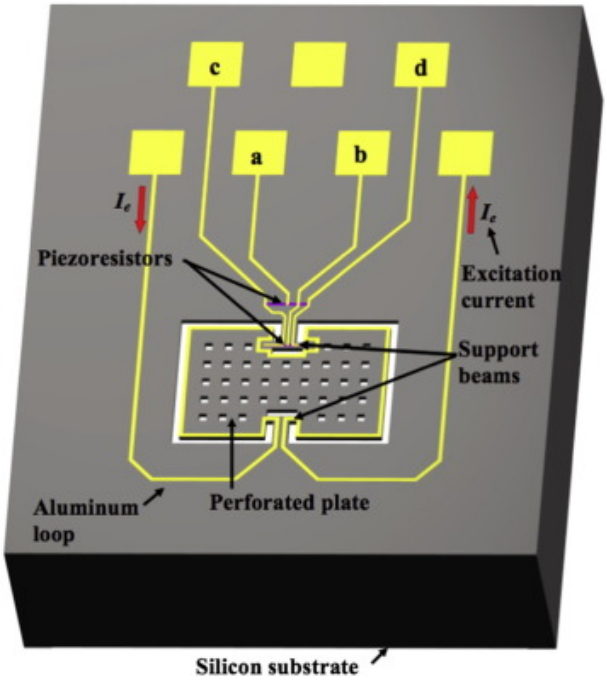


FIG. 5. A 3D schematic view of the magnetic field sensor[14].

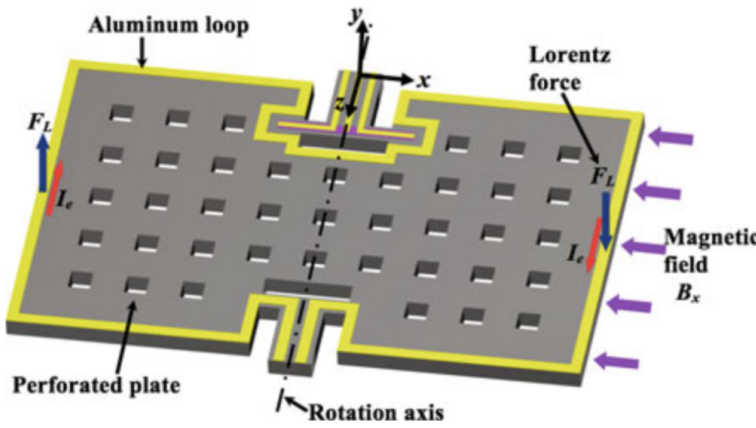


FIG. 6. Schematic view of the operation principle of a MEMS-based Lorentz force magnetometer[13]

where $\vec{F}$ is the Lorentz force acting on the wire; $\vec{I}$ is the current in the wire; $\vec{B}$ is the magnetic field through the wire.

The perforated plate will experience Lorentz Forces as shown in Fig. 6. The right hand rule reveals that only a magnetic field pointing in the x direction of our coordinate system will induce motion. Since the slab's motion is only observed for magnetic fields parallel to the x axis, we find that the Lorentz Force becomes:

$$F_L = I_e L_y B_x \tag{3}$$

where $I_e$ is the excitation current driven through the aluminum loop, and $L_y$ is the width of the silicon plate.

If the current $I_e$ is sinusoidal, then the magnitude of the Lorentz Force can be written as

$$F_L = I_{max} \sin(wt) L_y B_x \tag{4}$$

where the oscillating current has a max value of $I_{max}$ and has angular frequency $w$; $t$ is time. Eq. 4 indicates that the Lorentz force will oscillate corresponding to the undulations of the current in the wire. As a result, the silicon plate will oscillate like a "seesaw." In other words, the plate will bend along the central axis where the perforated plate connects to the large silicon substrate, and the extent at which the plate bends will be a function of the magnitude of the field in the x direction.

The sensor can quantify the extent of plate bending using a piezoresistor— a material whose electrical conductivity varies as a function of strain. Recall that strain is the deformation of an object, which we can quantify as the fractional change in length $\frac{\Delta L}{L}$ of the material subject to a force. Stress is force per unit area acting on the material. The strain on the device can be visualized in Fig. 7, which shows a cross section in the X-Y plane

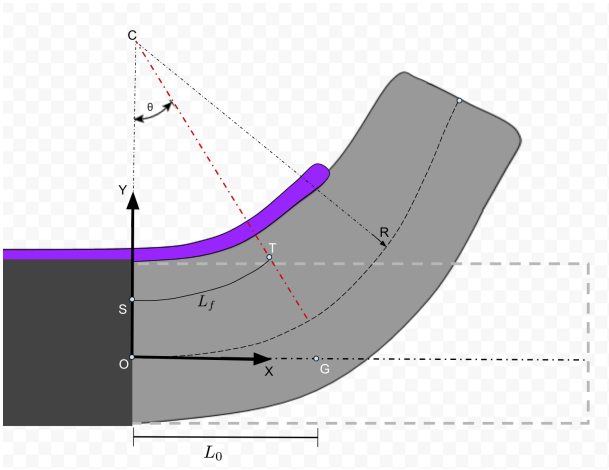


FIG. 7. Cross section of perforated plate in the X-Y plane. Segment OG and ST are the same length when the plate is not bending. As shown, however, OG and ST will not be the same length when the plate is bent by an external force.

of the bent perforated plate. The diagram provides an intuition for how the perforated plate will be strained.

Piezoresistivity arises from the fact that the energy bandwidth for a particular electron state is generally a function of inter-atomic spacing of a crystal structure, as shown in Fig. 8. Note that generally the closer the atoms are to each other, the greater the energy bandwidth will be. We can then show that the inter-atomic spacing of a material will affect the effective mass of conduction electrons, thereby affecting their mobility, which in turn affects the conductivity of the material. To examine how stressing a material can change a piezoresistor's resistance, recall that within a conduction band, electrons can be modeled as free particles with an effective mass, $m^*$. The minimum electron energy, $E(|\vec{k}|)$, in the

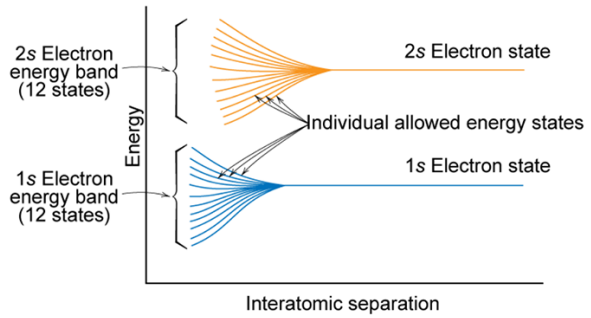


FIG. 8. Schematic plot of electron energy versus interatomic separation for an aggregate of 12 atoms. The 1s and 2s states split to form an electron band consisting of 12 states[15].

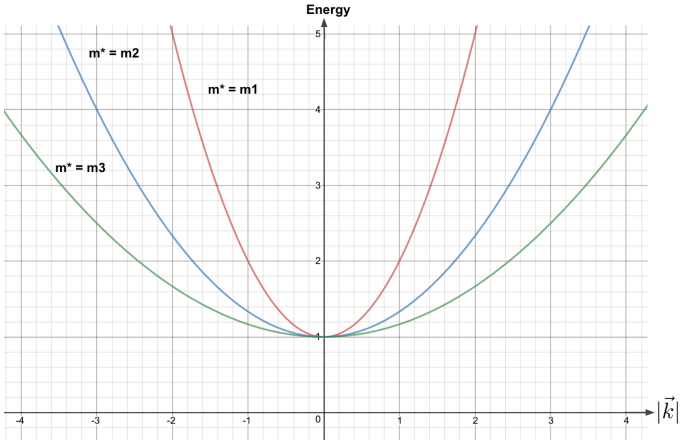


FIG. 9. Graph that conceptually depicts how changes to the bandwidth of an energy band corresponds to changes in the effective mass of an electron. Y axis is energy and X axis is magnitude of electron's wave vector.

conduction band can consequently be modeled as:

$$E(|\vec{k}|) = E_0 + \frac{\hbar^2|\vec{k}|^2}{2m^*} \tag{5}$$

where $\vec{k}$ is the wave vector of the electron, and $E_0$ is the lowest energy in the conduction band.

When a piezoresistor is strained, the inter-atomic spacing in the material will change, affecting the energy bandwidth as shown in Fig. 8. According to Eq. 5, the effective mass of the electrons must change in order to satisfy the changes in the bandwidth. Fig. 9 shows how different energy bandwidths correspond to particular values of the effective mass (m1, m2, m3) if we set: $E_0 = 1$; $\hbar = 1$. In summary, when stress induces a change in the inter-atomic spacing of a material, we expect the effective mass of electrons in the conduction band to change.

Next we can show that changes in effective mass of electrons in the conduction band will affect a material's conductivity. Recall that the conductivity, $\sigma$, of most materials can be approximated as:

$$\sigma = n|e|\mu_e \tag{6}$$

where n is the number of free electrons in the conduction band, $\mu_e$ is their mobility, and e is the charge of an

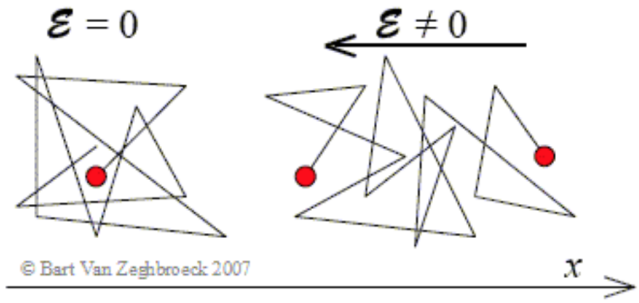


FIG. 10. Classical representation of the motion of a charged particle that collides with other particles (not shown in image). Left image is when electric field is not present. Right image is when electric field is present. In the right image, there is a net motion to the left, characterized by a drift velocity[16].

electron. Recall that mobility describes the net motion of electrons across a material and is defined as the drift velocity per unit electric field. Fig. 10 shows the net motion of a charged particle when the particle is subject to an electric field. The image provides an intuition for how conduction electrons are moving in the piezoresistor. From Newton's Second Law, we intuitively expect that charged particles with greater mass will have a greater inertial resistance to forces. Consequently, we can expect the mobility of a charged particle to be inversely proportional to the mass of the object[16].

In summary, when the piezoresistor is stressed, the inter-atomic spacing of a material will change, consequently affecting the effective mass of electrons within the conduction band. As a result, we expect the mobility of electrons to change, affecting the resistance of the piezoresistor. Therefore, a Lorentz Force Magnetometer can use the changes in the piezoresistor's resistance to quantify the stress on the device due to an external magnetic field. The device's piezoresistors are located on the support beams, which will bend due to the Lorentz Forces and therefore experience a strain. The piezoresistors are integrated in the device's circuit such that changes in the piezoresistor's resistance will be directly reflected in the output voltage.

We can show that the change in resistance in the piezoresistor will be linearly related to the magnetic field if we can argue that the strain the device experiences is very small. If strain is sufficiently small, we can first argue that 1) the piezoresistors resistance is linearly related to strain and 2) the device will exhibit linear elasticity (stress and strain are linearly related). A strain of 0.2 percent is generally accepted to be sufficiently below the limit at which linearity breaks down[17]. Although the accepted point of 0.2 percent is arbitrary, we can use it to determine whether we should be worried about nonlinearity between stress and strain. If we initially assume linear elasticity, we can use Hooke's law to obtain an approximation for the order of magnitude for strain:

$$\epsilon_x = \frac{\sigma_x}{E} \tag{7}$$

where $\sigma_x$ is the stress in the x direction. Recall that

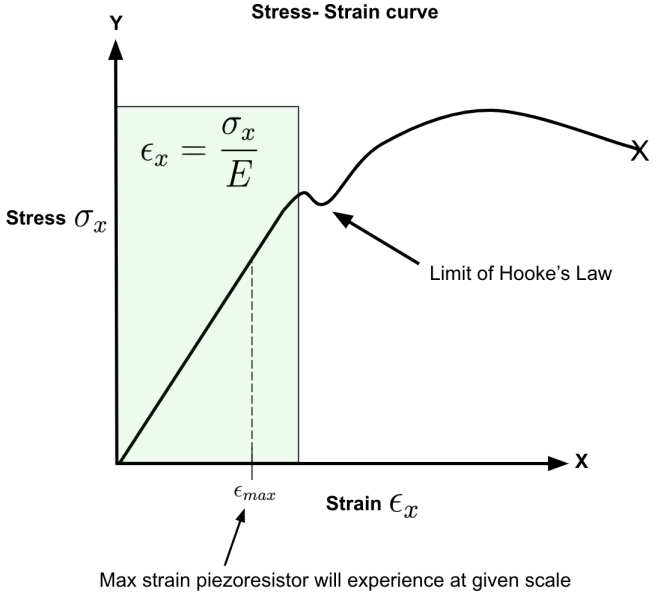


FIG. 11. Stress-Strain curve. $\epsilon_{max}$ is the max strain possibly induced by the Lorentz Force. This graph is for conceptual understanding, so units are omitted.

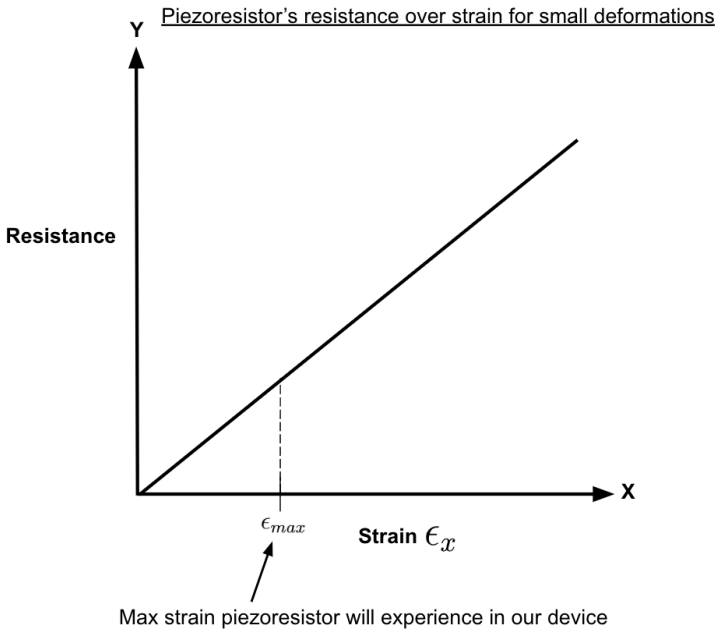


FIG. 12. Piezoresistance over strain for small deformations. This graph is for conceptual understanding, so units are omitted.

stress is defined as the magnitude of the offending force per unit of cross sectional area of the stressed object.

In our case, the Lorentz Force described by Eq. 3 will induce the stress on the device, so if we apply the definition for stress we find:

$$\sigma_x = \frac{I_e L_y B_x}{A} \tag{8}$$

where A is the cross sectional area of the support beam. Combining equation 7 and 8 further yields:

$$\epsilon_x = \frac{I_e L_y B_x}{AE} \tag{9}$$

We can examine the magnitude of the variables in Eq. 9 to approximate order of magnitude of strain. The dimensions of the support beams will be in the order of micrometers, so the cross sectional area will be in the order of square micrometers. Additionally, the excitation current $I_e$ will be in the range between 10-30mA, $L_y$ is 300 $\mu$m, and $B_x$ will be in the order of micro Tesla since the earth's magnetic field at the surface is on average 50 $\mu$T[18]. The support beam is primarily composed of silicon, which has an elastic modulus E between 130 GPa and 188 GPa[19]. These values yield a strain whose magnitude is in the order of $\approx 10^{-12}$. Therefore, strain will be much less than the yielding point of 0.2 percent (i.e. $\epsilon_x << .002$). Therefore linearity between strain and stress is a valid assumption— our device exists in the low strain regime, as depicted in Fig. 11 and as described by Eq. 7.

In addition, for sufficiently small deformations ($\epsilon_x << .002$), the piezoresistor's resistance and the induced strain will be linearly related, as shown in Fig. 12[14]. Therefore, we will observe the change in electrical resistance, $\Delta R$, and strain in the x direction, $\epsilon_x$, to be related as:

$$\Delta R \propto \epsilon_x \tag{10}$$

The next step in order to draw a relationship between output voltage and magnetic field is to relate stress to the magnetic field. Since stress is force per unit area on a body, we know that stress on piezoresistor will be proportional to the Lorentz Force. Combining Eqs. 4,7, and 10, we find:

$$\Delta R \propto B_x I_{max} \sin(\omega t) \tag{11}$$

The final step is to outline a relationship between electrical resistance of the piezoresistor and the output voltage. The piezoresistor is connected to a Wheatstone bridge, as shown in Fig. 13. The initial resistance $R_i$ varies by a certain amount, $\Delta R$, due to the piezoresistor. If $V_{in}$ is the voltage applied to the Wheatstone bridge, the changing resistance due to the Lorentz Force on the piezoresistors will change the output voltage of the Wheatstone bridge.

We can calculate the output voltage as a function of the change in resistance $\Delta R$ by treating the terminals b and a from Fig. 13 as individual voltage dividers, which results in the the following:

$$\frac{V_{out}}{V_{in}} = \frac{V_a - V_b}{V_{in}} = \frac{R_4}{R_3 + R_4} - \frac{R_2 - \Delta R}{R_1 + R_2} \tag{12}$$

If we simplify the above relationship by making the resistors equal to each other, we find

$$V_{out} = \frac{\Delta R}{2R_i} V_{in} \tag{13}$$

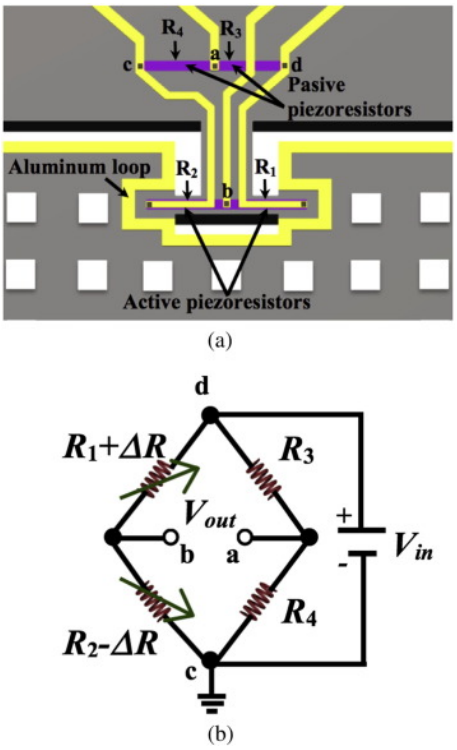


FIG. 13. Schematic view of the (a) piezoresistor and their electrical connections in the (b) Wheatstone bridge[14].

where $R_i$ is the initial resistance. If we combine the relationship 11 and Eq. 13, we find:

$$V_{out} \propto B_x I_{max} \sin(\omega t) V_{in} \tag{14}$$

Thus the output voltage and magnetic field in the x direction are linearly related.

In summary, the device is excited with a sinusoidal current through the aluminum trace on the perforated plate. Therefore, an external magnetic field in the x direction will produce Lorentz Forces that will cause the plate to bend. As the piezoresistor on the plate bends, the resistance in the device's circuit will change. After applying simplifying and valid assumptions, such as Hooke's law, the output voltage is found to be linearly related to the magnetic field.

The sensor thus described can detect magnetic fields in a single dimension. One could imagine measuring other components of the magnetic field with alternative orientations of the device.

### B. Vehicle detection using Magnetometers

Magnetometers can be designed to measure all three vector components of a magnetic field. For example, a system that contains multiple Lorentz Force Sensors at different spatial orientations could measure all desired components. Fig. 14 shows sample data of a three axis magnetometer, when a van passes over a sensor installed in a traffic lane. Three of the graphs represent how Earth's magnetic field varies with respect to a particular axis. Vehicles can create characteristic curves that

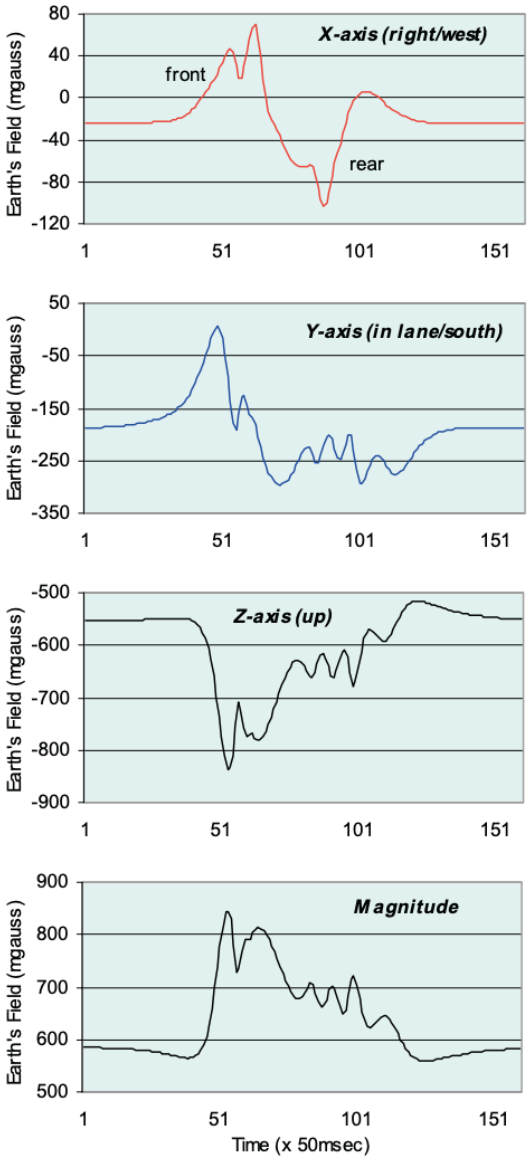


FIG. 14. Earth's field variations for a van driving over magnetometer. Vehicle is traveling south[12].

encode information about direction, vehicle speed, presence and vehicle type. Therefore, the encoded information can be extracted using modern computational and pattern recognition techniques[12].

To gain an intuition for these graphs, we can model magnetized vehicles as a simple dipole existing in a uniform magnetic field. At sufficiently small scales, the resulting vector field would resemble the one shown in Fig. 15. The dipole is located at the origin of the Cartesian coordinate system and our theoretical magnetometer is located at some value of Z below the origin. In this model, a magnetometer traveling West from the vehicle's perspective will measure the Z component of the magnetic field to initially decrease from the nominal value corresponding to Earth's magnetic field, then increase back to the nominal value, then decrease, and then finally increase once more. The experimental data shown in Fig.

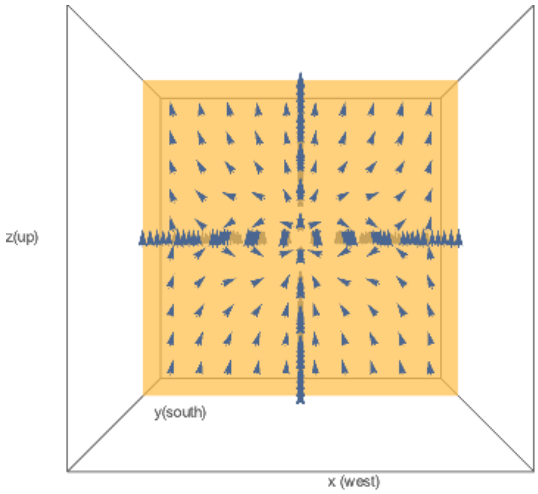


FIG. 15. Magnetic vector field that represents a magnetized vehicle in Earth's uniform field. The magnetic dipole that represents the car is at the origin. The field has a viewpoint that emphasizes the Z-X plane. The dipole's North is oriented in positive z.

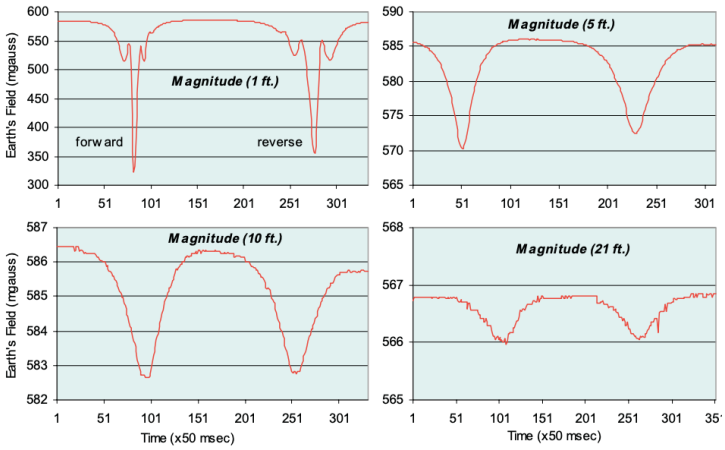


FIG. 16. Magnitude of magnetic field variations for a car traveling forward and reverse at distances 1, 5, and 10 feet (moving north-south) and 21 feet (moving east-west)[12].

14 (Z-axis) agrees that the measured magnetic field will initially decrease and then eventually increase— the end behavior is in agreement. However, it is difficult to explain the rest of the exhibited features using our simple dipole model. This affirms that vehicles are more complex than a simple dipole system, and consequently will exhibit more unusual measurement characteristics.

For smart parking services, one of the most useful applications of magnetometers is simply detecting vehicle presence above a parking spot. When a vehicle is directly above a sensor, the magnetometer will detect the greatest variation in the magnitude of Earth's magnetic field. As shown in Fig. 16, the sensor detects a significant change in earth's magnetic field when a vehicle is very close to the sensor (1ft), as opposed to when it is 5, 10 or 21 feet. This means that for a stationary parked car, there will generally be the greatest deviation of Earth's magnetic field when the car is directly above the sensor.

A wireless network of these sensors would provide high resolution measurements. A network of magnetic field sensors could estimate queue lengths, categorize types of vehicles, estimate traffic flow (vehicles/time), determine parking space availability, and more[20], which is valuable information that can be exploited for many applications.

## III. SENSOR INTEGRATION IN SMART GRID

The Smart Grid is the next evolution of the traditional power grid, and is a crucial component in smart cities[3]. The smart grid contains sensors that collect information on different aspects of the power grid to improve management and operational efficiency, and in this process achieves new standards in security and sustainability. Sensor information on production, transmission, and distribution of energy will enable new applications and services that can further improve operations and client experience. Smart Grids are anticipated to provide benefits such as predictive maintenance, self-healing responses to system disturbances, improved capacity, increased ability for integration of renewable energy sources, reduction in the need for oil consumption during peak demand, and much more[21].

The next sections focus on how data collection can help the transition from the traditional centralized generation scheme to the Smart Grid's mixed generation scheme that incorporates distributed energy sources and renewable energy sources. In particular, the paper will explore the Phase Measurement Unit (PMU) sensor and its applications.

### A. Background on Integrating Distributed Generation Sources

The power grid is becoming less centralized as it integrates distributed generation sources, such as photovoltaics and wind turbines. The integration, however, increases the physical stress of the system. Renewable Energies Sources often do not provide the same kind of stability provided by traditional sources of energy.

The traditional power grid is made up of an interconnected network of generators that work synchronously, hence the name synchronous generators. The kinetic energy stored in traditional generators is directly coupled to the energy consumed in the power grid. As a result, more massive generators can better support the grid during an imbalance between energy production and consumption, as opposed to less massive generators. Since traditional generators are interconnected and synchronized, the power grid is highly resistant to change due to the large inertial response of the generators, which is an important stabilizing feature of traditional grids during power imbalances. Once the disturbance occurs, the inertial response from the synchronous generators will provide enough time for operators to begin the primary control action, which takes about 10-30s to initiate[22]. Re-balancing the grid can involve stabilizing techniques

such as load shedding or engaging back up generators, depending on whether there is a stall or surge in the system.

Unfortunately, many distributed energy sources do not contribute to the inertia of the system, and as they replace synchronous generators, they reduce the inertia of the grid system provided by traditional technology. This makes the system fickle to disturbances[23]. For example, photovoltaics have no moving parts, and as a result provide no inertial stability to the grid. Similarly, wind turbines are variable, so they can't be directly connected to the power grid. Finally, Renewable Energy Sources often need a power converter to be integrated into a 50/60 Hz power grid, which electrically decouples the generator from the grid. This means that there is no longer a connection between any stabilizing inertia from the source and the grid[23]. These kinds of generation units are often called converter connected generation since they are connected to the grid via a power converter.

It is clear that the traditional grid's stability does not readily support the integration of distributed generation. Regardless, distributed generation is capable of replacing the stability provided by the inertia of fossil fuel-based turbines. The future of the grid is one in which bulk distributed generators and converter-connected generators provide sufficient stability to the grid during disturbances. Using real-time data on the state of the grid, distributed generators could mimic the inertial response that the traditional synchronous generators produce during an electrical disturbance, providing an effective stabilizing response[23]. This is particularly important for integrating large amounts of renewable energy sources into the power grid. Phase Measurement Units (PMUs) are sensors that can measure time-stamped voltages and phase angles of a signal and that can enable the mentioned solution for integrating renewable energy sources.[22].

### B. Supporting Frequency Stability with Frequency Sensors

In order to understand how sensors can be used to integrate renewable energy sources, it is informative to examine how the grid derives frequency stability from traditional generators. The stability of the grid frequency is directly related to the motion of the rotor in traditional generators. Fig. 17 shows a simplified schematic of a power plant. In general, a fuel source is used to heat up a gas or steam, which is used to drive the rotor of a turbine. The turbine's rotor is coupled with a generator, producing electricity for the grid to distribute to consumers. The input power from the fuel source is converted to mechanical power, dumping kinetic energy into the rotor every second, $P_{in} = \frac{dE_{in}}{dt}$. On the other hand, users are consuming energy, taking away kinetic energy from the rotor every second, $P_{load} = \frac{dE_{load}}{dt}$. If the input power onto the rotor and power consumed are equal to each other, the amount of energy dumped into the rotor will be equal to the amount taken away from the rotor, so the rotor's kinetic energy will remain constant.

The angular velocity of the rotor is directly proportional to the frequency in the grid. This can be intuitively observed in figure 18, which displays the cross section of a generator next to a timeseries of the voltage generated. The plus sign at the center of the left diagram represents the central axis of the rotor. In the shown diagram, the rotor consists of a dipole magnetic that rotates with the rotor at some angular velocity. In our simplified diagram, a coil is located below the symbol $t1$, and it is connected to the rest of grid. The magnetic flux passing through the area of the coil will change as the rotor's magnetic dipole rotates. From Faraday's Law, we expect the the changing magnetic flux to induce an electromotive force in the coil by:

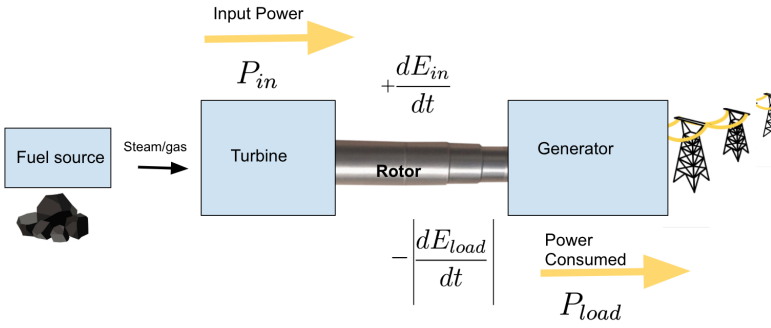


FIG. 17. Simplified schematic of power plant.

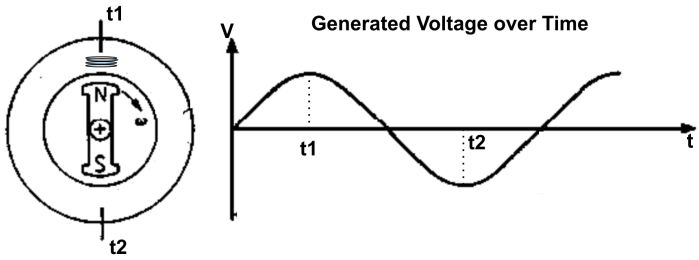


FIG. 18. Cross section of simplified generator[24].

$$v_{emf} \propto -\frac{d\Phi_B}{dt} \tag{15}$$

where $v_{emf}$ is the induced electromotive force, $\Phi_B$ is the magnetic flux through the magnetic coils. In other words, the frequency of the electromotive force in the coil is directly coupled with the angular velocity of the rotor. Therefore, changes in the speed of the rotor will consequently change grid frequency.

It is clear that the motion of the synchronous generator will reflect the balance between input power from power plant and power demanded from consumers, which will consequently affect the frequency of the grid. We can model synchronous generators using newton's second law for rotating objects.

$$J\frac{dw_r}{dt} = \tau_{input} - \tau_{load} \tag{16}$$

where

- $J$ is the moment of inertia of the rotor

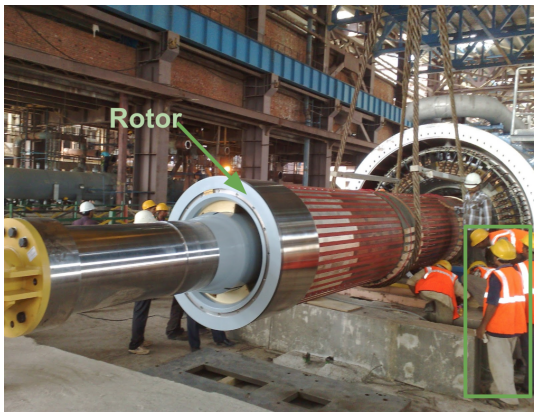


FIG. 19. Image of generic generator. Rotor is very massive and consequently has a large moment of inertia[25].

- $w_r$ is the angular velocity of the rotor
- $\tau_{input}$ is the mechanical torque on rotor due to input power
- $\tau_{load}$ is the electromagnetic torque on rotor due to power demand

Since variations in angular velocity from the rotor's nominal value $\omega_0$ will be very small, Eq. 16 can be rewritten as

$$\frac{dw_r}{dt} = \frac{P_m - P_e}{J\omega_r} \approx \frac{P_m - P_e}{J\omega_0} \tag{17}$$

where $P_m$ is mechanical input power on rotor, and $P_e$ is electromagnetic demand power on rotor.

From Eq. 17, it is clear that the rate of change of the rotor's angular velocity is inversely proportional to its moment of inertia. In other words, the more massive the rotor, the harder it is to change its angular velocity. The rotor's inertia will therefore help maintain the grid frequency at nominal value even when there are small power imbalances between input mechanical power and power demand. This is why utility generators are so large. Fig. 19 shows an example of what utility generators look like. A person is outlined for size comparison. These large traditional generators will greatly dampen any frequency deviations in the power grid.

Solar panels have no chance at providing similar natural stability— they have no moving parts that can be used to dampen frequency changes. In addition, the capacitive reactance of solar panels generally does not provide a sufficient stabilizing response, so alternative solutions are needed. On the other hand, wind turbines do have moving parts. However, since the turbine speed is variable, it will produce corresponding variable voltage frequencies. This cannot be connected directly to the grid, since the grid operates at a standard frequency value. As a result, wind turbines are connected via a converter, and are therefore electronically decoupled from the grid. In other words, the grid can't depend on the inertia of wind turbines for stability.

So how can sensors be used to integrate renewable energy sources? Frequency sensors can be used to measure the frequency of the grid, which encodes information about the power imbalance in the grid, as shown in Eq. 17. With appropriate control functions, real-time measurements of grid frequency can be used to determine how much power should be injected or withdrawn from the grid for stabilization. It should also be noted that renewable energy systems need external methods for quickly reducing or increasing energy output, such as battery storage.

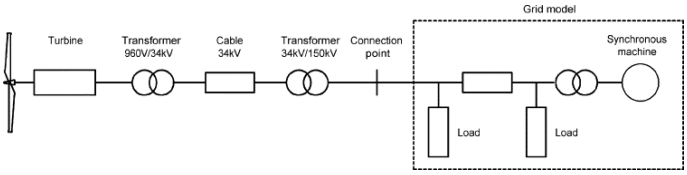


FIG. 20. Schematic for simplified grid used in simulation. Nominal voltage of grid is 13.8 kV; wind farm is connected to grid through a 34kV cable and 34kV/13.8kV transformer[26].

There are several methods for calculating the appropriate power to inject or withdraw from the grid. One method is by modeling renewable energy sources as if they were a traditional generators with a "virtual rotor." We would then be able to apply previously derived equations, such as 17, and see that the output power of the renewable energy source will be proportional to the virtual moment of inertia, $J_v$ and the rate of change of grid frequency $\frac{df_g}{dt}$.

$$P_{out} \propto J_v \frac{df_g}{dt} \tag{18}$$

where $P_{out}$ is the output voltage from a generator that supports grid stability.

This method has been shown and observed to work as desired. In one case study, wind turbines were able to effectively stabilize the grid during disturbances with a control function. In the simulation, a simplified grid is used as shown in Fig. 20. A 15MW wind farm is located to the left of the diagram. The two attached loads are 10MW and 90MW, so the initial load on the system is 100MW total. Suddenly, an additional 10MW load is added to the grid. As shown in Fig. 21, the frequency drops to about 49.7 Hz when the wind farm provides no stability for the grid, and the frequency drop is less when there is a control function in place.

In the United States, power plants have automatic response actions when the frequency varies more than .02 Hz. Deviations past .5 Hz require more intense response measures, such as "underfrequency load shedding," which is when power plants disconnect loads (i.e. neighborhoods, blocks, houses) from the grid[27]. As shown in Fig. 22, power plants generally begin load shedding around 1 Hz, at which point black outs can be anticipated.

### C. Phase Measurement Unit output

The results above are contingent on being able to measure the frequency of the grid in real-time. The Phase Measurement Unit (PMU) is a sensor that is being researched and implemented, partially motivated by the

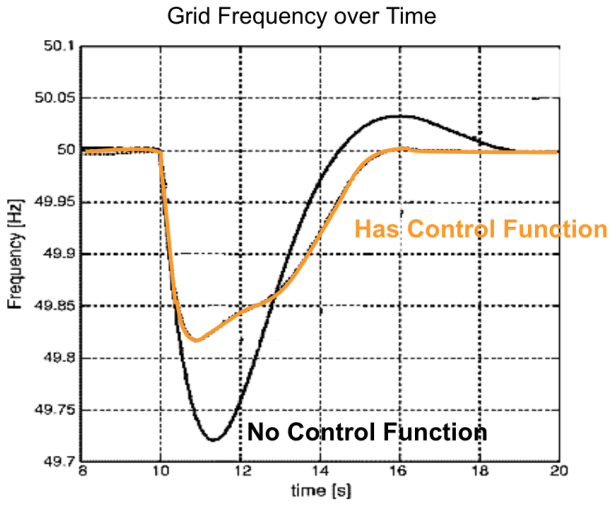


FIG. 21. The simulated grid frequency over time. Black line is trial when wind farm provides no inertial stability. Orange line is trial when wind farm provides virtual inertial stability with a control function[26]. The wind farm uses droop control for the simulation.

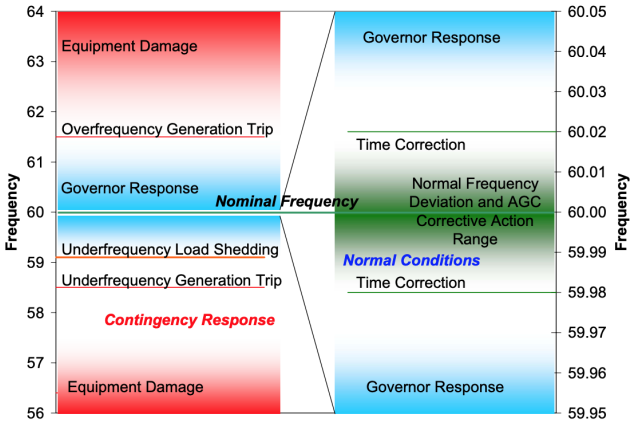


FIG. 22. Depicts power plant response actions for frequency deviations away from nominal(60 Hz). Underfrequency load shedding occurs at approximately 59 Hz.

North American SynchroPhasor Initative. The initiative has led to the installment of phase measurement units across the U.S., providing valuable data with many more applications than are explored in this paper. The next few paragraphs explore the basics of what a PMU is.

The PMU can measure time-stamped voltages and currents in a power system, and determine the corresponding phasor quantities. The device provides information on the magnitude of the phasor, as well as its phase angle, represented in Fig. 23. Recall that phasors are vectors in the complex plane, and in our case, the phasor contains information about phase and magnitude of voltage or current.

Mathematically phasors can be described as

$$\boldsymbol{V} = V_p[\cos(\phi) + i\sin(\phi)] = (V_p)e^{i\phi} \tag{19}$$

where:

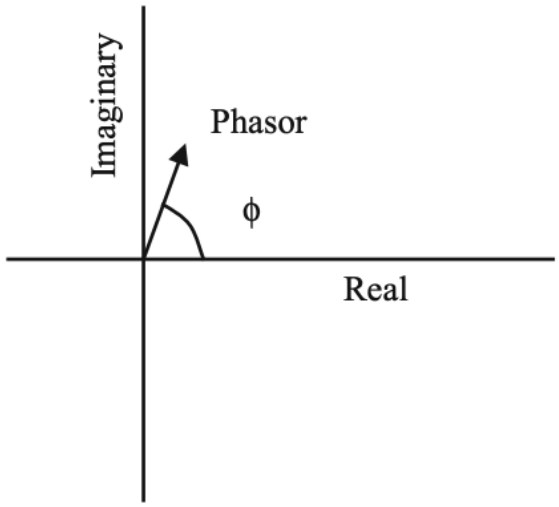


FIG. 23. Phasor diagram. The phase is the angle between a sample and the peak of the input signal, which corresponds to when the phasor is parallel to the real axis[13].

- $V_p$ = peak amplitude of signal
- $\phi$ = phase angle in radians

A single phase measurement unit can calculate voltage and current phasors at a particular location in the grid at a particular instant of time. When PMUs are organized in a network and synchronized using GPS, they provide synchronized phase measurements about the Grid's state, and are consequently called synchrophasors. Sample synchrophasor data is shown in Fig. 24. The figure provides synchrophasors for the grid in Colorado during normal operating conditions. The normal operating conditions are when the voltage and frequency are operating at the nominal values. In the United States, the nominal operational frequency is 60 Hz.

As Fig. 24 shows, the frequency in the grid varies within a window of ± .02 Hz. This variation during optimal operation is significantly less than critical values where mass generator tripping might be anticipated, such as when the frequency varies beyond ± .5Hz from nominal value[29]. The low variation during optimal hours reflects the reliability of the Colorado grid. However, as synchronous generators, along with their stabilizing inertial response, are replaced with converter-connected or solid state generators like photovoltaics, the system grid has a reduced inertial response. More specifically, reducing the inertial response of the grid system increases the grid's rate of change of frequency during a disturbance, which means that the grid destabilizes at quicker rates in lower inertia states. Without the use of virtual inertia, grid frequency can rapidly reach critical deviations during low inertia states.

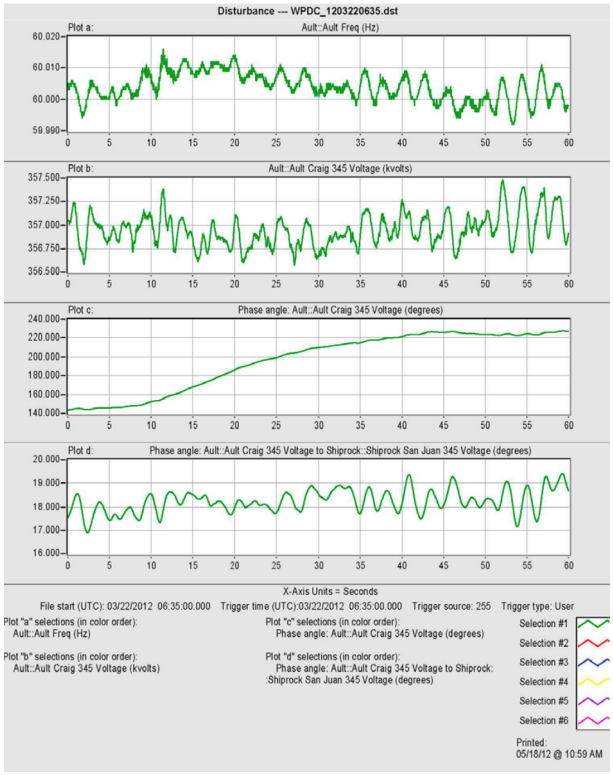


FIG. 24. Plot (a) shows the trace of frequency recorded by the Ault, Colorado PMU during a 1 min window. Plots (b) and (c) show the voltage magnitude and phase angle of the AultCraig, Colorado 345-kV line measured at Ault during the same 1-min window. Plot d shows the phase angle difference between the voltage phasors at Ault and Shiprock, New Mexico[28].

## IV. SENSOR APPLICATIONS FOR EARLY DETECTION OF NATURAL DISASTERS

Sensors can play an important role in early detection and monitoring of natural disasters (e.g. earthquakes, tornadoes, tsunamis, etc.) that threaten inhabited areas. The Indian Tsunami Early Warning System is an example of how a network of sensors (pressure sensors, satellites, accelerometers) can be used to determine where a tsunami will strike[30]. Other sensor systems, such as Grillo are used to evaluate structural stability of buildings after earthquakes, potentially saving people from buildings that are hazardous but appear safe. In the United States, sensor integration for the purpose of wildfire detection could save lives and prevent costs.

### A. Background: Detecting Wildfires with Sensors

There are several different methods of detecting wildfires. There are airborne, spaceborne, or terrestrial sensing systems. Traditional systems use satellite monitoring to keep track of wildfires. However, spaceborne detection methods suffer from several disadvantages, such as high uncertainty (1km), infrequent monitoring, interference from clouds[31]. There is a growing body of literature on airborne sensing techniques involving drones, since they could be an effective method for detecting early signs of fire and facilitating post-fire analysis. However, they currently have several disadvantages, such as high cost, required specialized personnel, and more. Finally, there is a substantial body of literature on ground-based sensing techniques since they can often be cost effective and accurate. Some common terrestrial sensing technologies for wildfire detection include: visible spectra cameras, infrared cameras, LiDar, and widespread wireless sensor networks. It should be noted that sensor networks often measure data such as temperature, humidity, C02 levels, etc. Visible spectra cameras have proven to be powerful sensors for detecting wildfires, as exhibited by commercial sensor nodes such as FireWatch, which uses gray scale images to accurately detect early warning signs. One of the most physically interesting sensor technologies with the potential to detect wildfires is the radio-acoustic sounding system (RASS). This sensor system has been historically recognized for its ability to accurately produce three dimensional temperature profiles of a region. Near real-time temperature profiles of a region could prove to be extremely useful for detecting early wildfires. The system has been shown to be suitable for detecting crown and surface fires, but not ground fires[32], especially since they provide higher spatial resolution for temperature profiles than standard meteorological techniques. The next section explores how RASS creates temperature and wind profiles.

### B. Radio Acoustic Sounding System

In general, RASS determines temperature profiles of a region using two measured quantities: wind velocities and the speed of sound as a function of space. RASS measures wind velocities using standard wind profiling techniques. RASS measures the speed of sound using a doppler radar and an acoustic source. In order to understand how RASS measures the speed of sound, it is useful to understand how doppler radars work.

Consider a police radar gun. As shown in Fig. 25, the electromagnetic waves emitted by the radar gun will have a wavelength $\lambda$. Since the car is moving towards the police car, the reflected waves will be doppler shifted. The doppler shift will be be a function of velocity of the incident object, and can be expressed as:

$$\frac{\Delta f}{f_0} = \frac{v_{target}}{c} \tag{20}$$

where $\Delta f$ is the change in frequency, $v_{target}$ is the velocity of the moving object, and $f_0$ is the initial frequency of the electromagnetic wave.

If the frequency of the reflected wave is measured, then in principle the velocity of the incident object can be determined. Eq. 20 assumes that the moving object's velocity is perpendicular to the wave front of the electromagnetic (EM) wave. The calculation becomes more nuanced when objects are moving at different angles from the wave front, but the principle for determining velocity remains the same.

Similar to how EM waves can reflect from solid objects, EM waves can also reflect from density variations

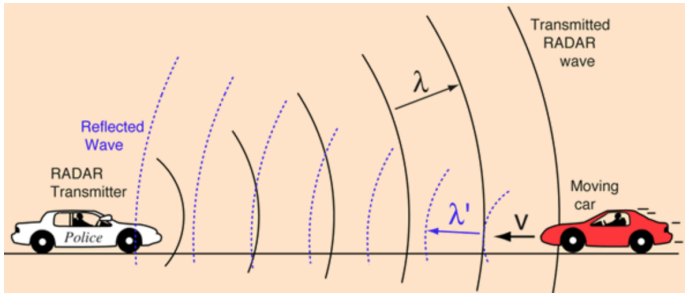


FIG. 25. Doppler shift of a police radar gun[33]

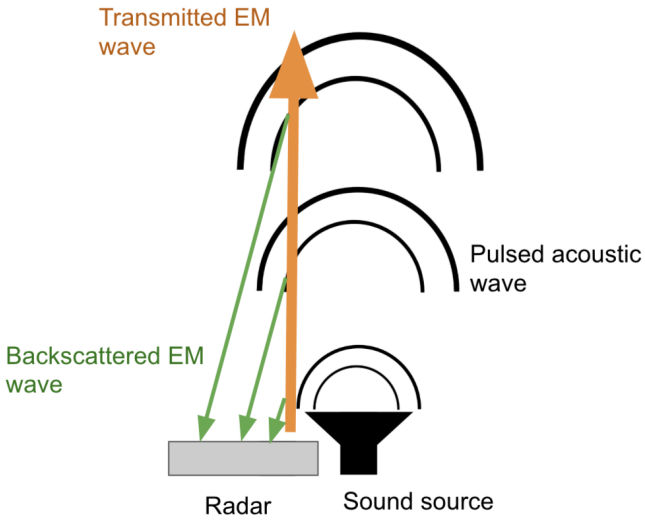


FIG. 26. RASS set up for measuring speed of sound. System measures reflected signal of a continuous electromagnetic wave incident on a pulsed acoustic wave.

in the air. RASS uses this principle to measure the speed of sound. As shown in Fig. 26, RASS measures the reflected signal of a continuous emitted electromagnetic wave incident on a pulsed acoustic wave, which produces measurable undulations in the density of the air. The acoustic wave effectively acts as a "moving vehicle," as if it were moving up to the sky whose velocity can be measured by the radar system.

The density undulations in the air will make the electromagnetic wave backscatter different amounts. This means that we can determine whether the electromagnetic (EM) wave reflected off the acoustic wave's peak or trough based on the magnitude of the backscattered signal. The backscattered signal will be obtained as data points in a time series. Each data point will have a corresponding measurement for doppler shift of the backscattered EM wave, which can be used to determine the speed of the acoustic wave using Eq. 20. As a result, the speed of the wave as a function of time can be determined. If we assume that the speed of light is constant in the relevant portions of the atmosphere, we can then use basic kinematics to determine the wave speed as a function of space. It should be noted that the undulations in air density are sufficiently small that the speed of light remains approximately constant at the desired level of sensitivity.

In summary: to measure the speed of sound, the acoustic source will emit pulsed sound waves. As the acoustic source does this the doppler radar will continuously emit electromagnetic waves to measure the speed of the emitted acoustic wave. To obtain velocity resolution for multiple dimensions, the device needs to repeat the process described above at different orientations simultaneously.

Once the speed of sound is measured as a function of distance, we need to somehow relate it to temperature to obtain the desired profile. Sound is a longitudinal wave, and the speed of a longitudinal wave behaves as:

$$C_L = \sqrt{\frac{B}{\rho}} \tag{21}$$

where $C_L$ is the speed of a longitudinal wave, B is the bulk modulus and $\rho$ is the density of the medium. The bulk modulus is a value used to describe a medium's elasticity— it is analogous to the spring constant of a spring.

As one would expect, the speed of sound depends on the properties of the medium according to Eq. 21. However, we are interested in the speed of sound as a function of the medium's temperature as opposed to density.

If we model air as an ideal gas, we can use the ideal gas law to relate density to temperature:

$$PV = nRT \tag{22}$$

where

- P = pressure
- V = volume
- n = number of moles
- R = ideal gas constant
- T = absolute temperature of gas

To model air as an ideal gas, we make some major assumptions: 1) all molecular interactions in air are due to collisions as opposed to attractive or repulsive forces; 2) all collisions are perfectly elastic so kinetic energy of the wave is preserved. For an ideal gas, the bulk modulus is:

$$B = \gamma P \tag{23}$$

where $\gamma$ is the heat capacity ratio.

We can combine Eqs. 21, 23, and 22 and find:

$$c_s = \sqrt{\frac{\gamma R}{M}}\sqrt{T} = k\sqrt{T} \tag{24}$$

where $c_s$ is speed of sound, M is molar mass, and k = $\sqrt{\frac{\gamma R}{M}}$, where k will change depending on humidity.

Some RASS can measure the humidity of the atmosphere as a function of space. However, in practice, measuring humidity can be difficult. As a result, some RASS

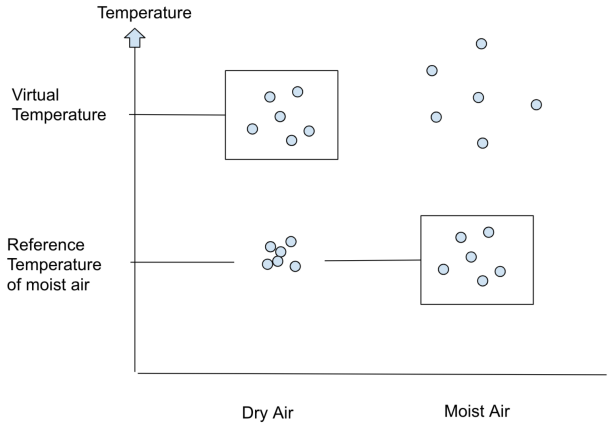


FIG. 27. Diagram exhibiting definition of virtual temperature. The circles represent air particles.

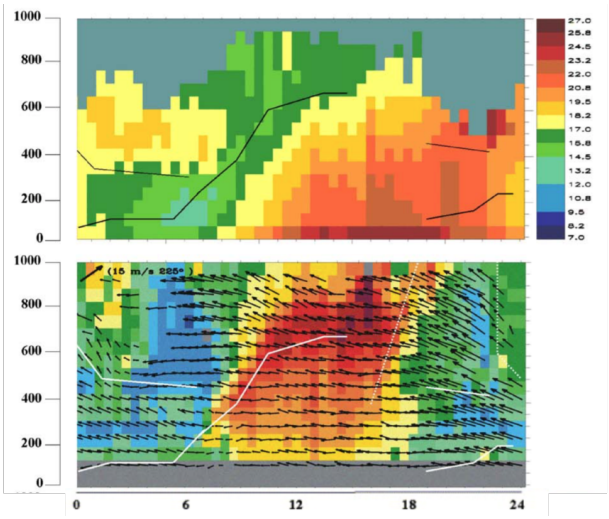


FIG. 28. Top graph shows temperature profile in which color represents temperature in celsius. Bottom graph shows horizontal wind vector field superimposed ontop of a color graph in which color represents level of electromagnetic backscattering. Y axis: meters above the planetary surface. The X axis: time in UTC. Data is chunked into one hour chunks[34].

approximates the atmosphere as dry. Consequently, the calculated value for temperature is no longer absolute temperature, but the temperature of a dry atmosphere, dubbed the virtual temperature $T_v$.

Virtual temperature is the temperature at which dry air is the same density as moist air, under constant pressure. Fig. 27 visually exhibits the definition. Since dry air is more dense than moist air, dry air will require higher temperatures to reach the reduced density of moist air. This is because under constant pressure, increases in temperature will naturally cause air particles to spread apart, because of the increase in kinetic energy. This is reflected in the relationship between virtual acoustic temperature and regular temperature, $T_v$ and $T$ respectively[34]:

$$T_v = T(1 + .51q) \tag{25}$$

where q is the moisture content by mass. Virtual temperature will always be greater than regular temperature depending on moisture content.

Since early wildfires will affect virtual temperature profiles comparably to absolute temperature, virtual temperature is sufficient for the purpose of detecting wildfires. We ultimately obtain:

$$c_s = k\sqrt{T_v} \tag{26}$$

Equation 26 draws a relationship between speed of sound and temperature when there is no wind flow. Since the lowest part of the atmosphere, also called the atmospheric boundary layer, experiences a lot of turbulence partially due to the unstratified distribution of temperature, moisture, etc, the sensor system will measure the sound wave's effective velocity, $c_{eff}$, which will be the vector sum of wind velocity $\vec{v_w}$ and the emitted wave velocity during no wind:

$$\vec{c_{eff}} = c_s\vec{n} + \vec{v_w} \tag{27}$$

where $\vec{n}$ is the unit vector normal to the front of the acoustic wave, and $c_{eff}$ is the measured effective velocity.

Since the effective velocity, of the acoustic wave can be determined with radar, all that is needed to determine the virtual temperature is the vector field of wind velocity, as shown in equation 27. Once again, the RASS system uses radar to create a wind velocity profile. The emitted electromagnetic waves will collide with moving wind, producing a backscattered signal that is Doppler shifted. The amount shifted can be used to determine the wind velocity.

The RASS system can therefore create virtual temperature and wind profiles for a region. Sample data is presented in Fig. 28. The top figure uses color to show temperature at different vertical heights. The bottom graph depicts horizontal wind speeds at different vertical heights. In addition, it uses color to show backscatter levels at different heights, which result from miscellaneous variations in atmospheric density. The x axis for both graphs is time in UTC, binned into one hour bins.

### C. Detecting Wild Fires

RASS data is useful because it 1) provides accurate temperature profiles that can be used to detect early fires 2) provides wind vector fields that can be used for predicting the fire path, allowing early deployment of fire control techniques. Accurate information on early fire detection and predictions of fire propagation can greatly mitigate the consequences of wildfires.

In practice, pattern recognition algorithms can be used for sophisticated detection systems. For first order approximations, sudden or characteristic changes in the temperature profiles of a region can be used to detect early wildfires. Automatic alerts could be set up when characteristic changes occur. Although RASS can provide meaningful data for wildfire detection, it should be

noted that the technology for this particularly purpose has not been widely studied within literature. In addition, it is one of the more costly detection systems, on par with LiDar, IR, and other camera sensors, since it requires look out towers and emergent technology[32]. It also produces a potentially loud noise which could impact the surrounding wildlife in unexpected ways. Powerful alternatives that are indeed further researched and more cost effective include wireless sensor networks and gray scale cameras. The most appropriate detection methods will depend on the structure of the forest and additional relevant parameters.

## V. CONCLUSION

Synergy between data collection, algorithms, and communication can help cities combat pressing global issues, including devastating natural disasters, changing energy production portfolio, and transportation inefficiency.

1) In particular, the U.S. department of transportation has made clear that parking and inefficient traffic lights are significant contributors to traffic congestion and therefore transportation emissions. Wireless sensor networks using magnetic field sensors can provide the necessary data for vehicle detection, enabling several meaningful solutions that could target significant portions of greenhouse gas emissions in transportation. In particular, vehicle detection enables smart parking and optimized traffic lights. The Lorentz Force Magnetic Field Sensor is one kind of magnetic field sensor that could be used in a wireless sensor network. The Lorentz Force Sensor makes use of several physical and engineering principles: a) ferromagnetic components of vehicles will be magnetized due to Earth's magnetic field; b) silicon's conductivity will change considerably when strained; c) the circuit is built such that nearby magnetic fields can induce a Lorentz Force that bends internal structures of the device, which can be quantified using the piezoresistive properties of silicon. The device's piezoresistors are connected to the rest of the circuit such that they will considerably affect the output voltage when strained, and as a result the sensor is able to measure the presence and motion of nearby vehicles. The sensor reveals many interesting topics, including ferromagnetism, electronics, band theory, and more.

2) The US Department of Energy has identified electricity production as the second largest contributor to GHG emissions, and has identified the need to integrate renewable energies. Unfortunately, renewable energy sources do not provide the same stability that traditional generators provide. However, sensor data, such as real time grid frequency measurements, allow renewable energy systems to inject or withdraw power from the grid as necessary in order to maintain frequency stability. Phase data can be obtained using wireless sensor networks, particularly using the Phase Measurement Unit. The process of using data to integrate renewable energy sources requires analysis involving energy flow in power systems, classical mechanics, advanced scenario modeling, and more.

3) The United States is haunted by devastating and worsening natural disasters. Wireless sensor networks can be used to help prevent natural disasters, particularly wildfires. Sensors, such as cameras, temperature sensors and RASS, can be used in a wireless sensor network for such an application. In particular, RASS provides two important pieces of data that can enable detection: wind and temperature profiles. In combination with pattern recognition algorithms and automated alerting schemes, crown and surface fires can be localised using temperature profiles, and their paths can be predicted using wind flow profiles. The sensor system makes use of several physical and engineering topics, including longitudinal wave behavior in gas mediums, state analysis of ideal gases, and radar technology. Although RASS is promising in theory and physically interesting, it may not be practical since it can be costly, require specialized personnel, and be audibly unpleasant.

Cybersecurity and privacy were out of the scope of this paper, but are very important considerations regarding sensor-based solutions. This domain of solutions requires thorough examination of privacy and cybersecurity, and are a critical component of a safe connected society. It should be noted that the importance of security is fortunately a prevalent theme within literature on sensor-based solutions.

Gathering meaningful data— whether through wireless sensor networks, crowdsensing, or vehicle communication— is an important and arguably critical step for cities and global society. Data-based solutions can enable many city improvements, such as 1) data-informed urban planning, 2) vehicular and pedestrian safety 3) improved transportation system 4) efficient public utilities, 5) improved natural disaster prevention, 6) reduced carbon footprint, and 7) increased operational efficiency. Ultimately this domain of solutions provides a viable pathway for creating a future in which people can breath city air without a moment doubt, where urban planners can design roads not just for reducing rush hour traffic, but for everyone— cyclists, children, elderly and drivers— and in which younger generations have the chance to build a society for an even more distant future.

## VI. ACKNOWLEDGEMENTS

Sincere thanks to all the people that have helped me engage with this material, such as Martha Larson, Jeff Walter, Barry Costanzi.

[1] *Minneapolis is growing at its fastest rate since 1950* (2018), URL: https://www.minnpost.com/politics-policy/2018/05/minneapolis-growing-its-fastest-rate-1950/

ANNOTATION: Provided information on growth rate in Minneapolis.

[2] *68 percent of the world population projected to live in urban areas by 2050, says UN — UN DESA Department of Economic and Social Affairs*, URL: https://www.un.org/development/desa/en/news/population/2018-revision-of-world-urbanization-prospects.html

ANNOTATION: Provided statistics on global population growth.

[3] E. Al Nuaimi, H. Al Neyadi, N. Mohamed and J. Al-Jaroodi, *Applications of big data to smart cities*, Journal of Internet Services and Applications **6** (2015) (1), p. 25

ANNOTATION: Described applications and benefits of sensor data.

[4] Inrix, *INRIX Global Traffic Scorecard*, URL: http://inrix.com/scorecard/

ANNOTATION: Provided statistics on transportation and traffic.

[5] *How air pollution can cause cancer* (2019), URL: https://www.cancerresearchuk.org/about-cancer/causes-of-cancer/air-pollution-radon-gas-and-cancer/how-air-pollution-can-cause-cancer

ANNOTATION: Correlated air pollution and illnesses.

[6] *Adaptive Traffic Lights* (2018)

[7] Ž. Bačić, T. Jogun and I. Majić, *Integrated Sensor Systems for Smart Cities*, Tehnički vjesnik **25** (2018) (1), pp. 277–284

ANNOTATION: Provided overview of how sensors can be used to build smart cities.

[8] *Smart City Challenge*, URL: https://www.transportation.gov/sites/dot.gov/files/docs/SmartCityChallengeLessonsLearned.pdf

ANNOTATION: Provided traffic delay facts.

[9] T. Lin, H. Rivano, F. Le Mouël, B. Baron, P. Spathis, H. Rivano, M. D. de Amorim, D. Coudert, S. Pérennes, H. Rivano *et al.*, *A survey of smart parking solutions*, parking **1524** (2017), p. 9050

ANNOTATION: Provided comprehensive survey of sensors used in parking applications.

[10] S. Y. Cheung, S. C. Ergen and P. Varaiya, *Traffic surveillance with wireless magnetic sensors*, in *Proceedings of the 12th ITS world congress* (2005), vol. 1917, p. 173181

ANNOTATION: Described how magnetometers can be used in traffic management.

[11] *Magnetic Field of the Earth*, URL: http://hyperphysics.phy-astr.gsu.edu/hbase/magnetic/MagEarth.html

ANNOTATION: Provided image of earth's magnetic field.

[12] M. J. Caruso and L. S. Withanawasam, *Vehicle Detection and Compass Applications using AMR Magnetic Sensors* (1999)

ANNOTATION: Provided data and analysis of how magnetometers can be used in detecting vehicles.

[13] *HIGH SENSITIVITY MAGNETOMETERS* (SPRINGER, 2018)

ANNOTATION: Book described kinds of magnetometers and relevant analysis.

[14] A. Herrera-May, M. Lara-Castro, F. López-Huerta, P. Gkotsis, J.-P. Raskin and E. Figueras, *A MEMS-based magnetic field sensor with simple resonant structure and linear electrical response*, Microelectronic Engineering **142** (2015), pp. 12–21

ANNOTATION: Important paper that revealed physics of Lorentz Force Magnetometer.

[15] W. D. Callister and D. G. Rethwisch, *Materials science and engineering: an introduction* (Wiley, 2018)

ANNOTATION: Provided overview to materials.

[16] B. V. Zeghbroeck, *Principles of Semiconductor Devices* (Prentice Hall, 2010)

ANNOTATION: Described physics of conduction electrons

[17] *Offset Yield Method*, URL: http://www.engineeringarchives.com/les_mom_offsetyieldmethod.html

ANNOTATION: Described concepts behind material yield.

[18] *Earth's Magnetic Field*, URL: https://sites.fas.harvard.edu/~scidemos/Geophysics/EarthsMagneticField/EarthsMagneticField.html

ANNOTATION: Described properties of Earth's Magnetic Field.

[19] J. Kim, D.-i. D. Cho and R. S. Muller, *Why is (111) silicon a better mechanical material for MEMS?*, in *Transducers 01 Eurosensors XV* (Springer, 2001), pp. 662–665

ANNOTATION: Described piezoresistor properties, including elastic modulus.

[20] A. Pascale, M. Nicoli, F. Deflorio, B. Dalla Chiara and U. Spagnolini, *Wireless sensor networks for traffic management and road safety*, IET Intelligent Transport Systems **6** (2012) (1), pp. 67–77

ANNOTATION: Described applications and benefits of wireless sensor networks for safety.

[21] X. Fang, S. Misra, G. Xue and D. Yang, *Smart Grid The New and Improved Power Grid: A Survey*, IEEE Communications Surveys Tutorials **14** (2012) (4), pp. 944–980

ANNOTATION: Provided comprehensive survey of the issues and benefits of transitioning to a smart grid

[22] U. Tamrakar, D. Shrestha, M. Maharjan, B. Bhattarai, T. Hansen and R. Tonkoski, *Virtual inertia: Current trends and future directions*, Applied Sciences **7** (2017) (7), p. 654

ANNOTATION: Important paper that described state of the art methods for providing virtual inertia as well as future methods.

[23] P. Tielens and D. V. Hertem, *The relevance of inertia in power systems*, Renewable and Sustainable Energy Reviews **55** (2016), pp. 999 – 1009, URL: http://www.sciencedirect.com/science/article/pii/S136403211501268X

ANNOTATION: Provided detailed analysis of why examining inertia is important for grid stability.

[24] *Synchronous Generators I*, URL: http://www.egr.unlv.edu/~eebag/SynchronousGeneratorI.pdf

ANNOTATION: Provided image of cross section of generator.

[25] D. Guha, *ABC OF THERMAL POWER PLANT* (1970), URL: http://dguha1952.blogspot.com/2014/07/erection-sequence-and-plan-for_30.html

ANNOTATION: Described physics of power plants.

[26] J. Morren, J. Pierik and S. W. De Haan, *Inertial response of variable speed wind turbines*, Electric power systems research **76** (2006) (11), pp. 980–987

ANNOTATION: Provided image of wind turbine simulation.

[27] *Maintaining Reliability in the Modern Power System* (2016), URL: https://www.energy.gov/sites/prod/files/2017/01/f34/MaintainingReliabilityintheModernPowerSystem.pdf

ANNOTATION: Described the importance and seriousness of frequency deviations.

[28] E. Muljadi, Y. Zhang, A. Allen, M. Singh, V. Gevorgian and Y. Wan, *Synchrophasor Applications for Wind Power Generation*, Tech. rep., National Renewable Energy Lab.(NREL), Golden, CO (United States) (2014)

ANNOTATION: Describes applications of Phase Measurement Units.

[29] A. Ulbig, T. S. Borsche and G. Andersson, *Impact of low rotational inertia on power system stability and operation*, IFAC Proceedings Volumes **47** (2014) (3), pp. 7290–7297

ANNOTATION: Provided information on how inertia impacts frequency stability in grid.

[30]N. Mohamed and J. Al-Jaroodi, *Real-time big data analytics: Applications and challenges*, in *High Performance Computing & Simulation (HPCS), 2014 International Conference on* (IEEE, 2014), pp. 305–310

ANNOTATION: Provided great information on the domains in which data analytics can impact, and it helped provide initial framework for the paper.

[31]G. Sakr, R. Ajour, A. Khaddaj, B. Saab, A. Salman, O. Helal, I. Elhajj and G. Mitri, *Forest fire detection wireless sensor node*, Parte: http://hdl. handle. net/10316.2/34013 (2014)

ANNOTATION: Provides analysis of how Wireless Sensor Networks can be used to detect wildfires.

[32]Y. G. Sahin and T. Ince, *Early forest fire detection using radio-acoustic sounding system*, Sensors **9** (2009) (3), pp. 1485–1498

ANNOTATION: Provides info on how RASS can be used to detect wildfires.

[33]*Police Radar*,
URL: `http://hyperphysics.phy-astr.gsu.edu/hbase/Sound/radar.html`

ANNOTATION: Described physics of doppler radar.

[34]S. Emeis, C. Münkel, S. Vogt, W. J. Müller and K. Schäfer, *Atmospheric boundary-layer structure from simultaneous SODAR, RASS, and ceilometer measurements*, Atmospheric Environment **38** (2004) (2), pp. 273–286

ANNOTATION: Described physics of RASS.

[35]

[36]

[37]*Frequency Control Concerns In The North American Electric Power System*

ANNOTATION: Described the control responses to frequency deviations.

[38]S. E. Bibri, *The IoT for smart sustainable cities of the future: An analytical framework for sensor-based big data applications for environmental sustainability*, Sustainable Cities and Society **38** (2018), pp. 230–253

ANNOTATION: Provided information on how data can impact cities.

[39]N. Lu, N. Cheng, N. Zhang, X. Shen and J. W. Mark, *Connected vehicles: Solutions and challenges*, IEEE internet of things journal **1** (2014) (4), pp. 289–299

ANNOTATION: Discussed connected vehicles as IoT sustainability solution.

[40]S. Al-Sultan, M. M. Al-Doori, A. H. Al-Bayatti and H. Zedan, *A comprehensive survey on vehicular ad hoc network*, Journal of network and computer applications **37** (2014), pp. 380–392

ANNOTATION: Provided information on how vehicles can transmit their data.

[41]*Concept of Operations for the Connected Vehicle Environment*,
URL: `https://smart.columbus.gov/uploadedFiles/Projects/SmartColumbusConceptofOperations-ConnectedVehicleEnvironment.pdf`

ANNOTATION: Described smart city initiatives in the US.

[42]*History of Intelligent Transportation Systems*,
URL: `https://www.its.dot.gov/history/index.html`

ANNOTATION: Described history of intelligent transportation systems.

[43]*The Smart City Challenge*,
URL: `https://www.its.dot.gov/communications/its_factsheets.htm`

ANNOTATION: Summarized findings from US Smart City initiative.

[44]S. E. Bibri and J. Krogstie, *The core enabling technologies of big data analytics and context-aware computing for smart sustainable cities: a review and synthesis*, Journal of Big Data **4** (2017) (1), p. 38

ANNOTATION: Provided information on state of the art data sensing in the context of sustainability.

[45]J. Miller, *Vehicle-to-vehicle-to-infrastructure (V2V2I) intelligent transportation system architecture*, in *Intelligent Vehicles Symposium, 2008 IEEE* (IEEE, 2008), pp. 715–720

ANNOTATION: Provided information about future of intelligent transportation systems and the current architecture.

[46]C. Englund, L. Chen, A. Vinel and S. Y. Lin, *Future applications of VANETs*, in *Vehicular ad hoc Networks* (Springer, 2015), pp. 525–544

ANNOTATION: Provided detailed description of application of vehicular communication.

[47]S. Djahel, R. Doolan, G.-M. Muntean and J. Murphy, *A communications-oriented perspective on traffic management systems for smart cities: Challenges and innovative approaches*, IEEE Communications Surveys & Tutorials **17** (2015)

ANNOTATION: Provided information on current challenges in traffic management.

[48]M. Raya and J.-P. Hubaux, *Securing vehicular ad hoc networks*, Journal of computer security **15** (2007) (1), pp. 39–68

ANNOTATION: Described the architecture of an intelligent transportation system.

[49]Y. Toor, P. Muhlethaler, A. Laouiti and A. De La Fortelle, *Vehicle ad hoc networks: Applications and related technical issues*, IEEE communications surveys & tutorials **10** (2008) (3), pp. 74–88

ANNOTATION: Provided information on technical issues that could hinder communication in Intelligent Transportation Systems.

[50]A. Ashtaiwi, *Vehicle Ad Hoc Networks* (2013),
URL: `https://www.youtube.com/watch?v=i2nGSUx9r_s`

[51]M. Eltoweissy, S. Olariu and M. Younis, *Towards autonomous vehicular clouds*, in *International Conference on Ad Hoc Networks* (Springer, 2010), pp. 1–16

ANNOTATION: Really great video describing how VANET communication works and the societal benefits.

[52]A. L. Herrera-May, F. López-Huerta and L. A. Aguilera-Cortés, *MEMS Lorentz Force Magnetometers*, in *High Sensitivity Magnetometers* (Springer, 2017), pp. 253–277

ANNOTATION: Important book that described the circuitry, physics and applications of magnetometers.

[53]D. Zografos and M. Ghandhari, *Estimation of power system inertia*, in *2016 IEEE Power and Energy Society General Meeting (PESGM)* (2016), pp. 1–5

ANNOTATION: Provided information on how PMUs can be used to estimate grid inertia in Britain.

[54]L. Sánchez, I. Elicegui, J. Cuesta, L. Muñoz and J. Lanza, *Integration of utilities infrastructures in a future internet enabled smart city framework*, Sensors **13** (2013) (11), pp. 14438–14465

ANNOTATION: Described the concept of adaptive traffic lights.

[55]P. M. Ashton, C. S. Saunders, G. A. Taylor, A. M. Carter and M. E. Bradley, *Inertia Estimation of the GB Power System Using Synchrophasor Measurements*, IEEE Transactions on Power Systems **30** (2015) (2), pp. 701–709

ANNOTATION: Described how synchrophasor applications can impact the grid.

[56]A. Muzhikyan, T. Mezher and A. M. Farid, *Power System Enterprise Control With Inertial Response Procurement*, IEEE Transactions on Power Systems **33** (2018) (4), pp. 3735–3744

ANNOTATION: Described how inertial response can be used to control the power grid.